Available online at www.sciencedirect.com
SCIENCE DIRECT
Journal of Molecular Graphics and Modelling 23 (2005) 524–536
Journal of Molecular Graphics and Modelling
www.elsevier.com/locate/JMGM

Molecular dynamics simulations for selection of kinetic hydrate inhibitors

Bjørn Kvamme *, Tatyana Kuznetsova, Kjetil Aasoldsen

Department of Physics, University of Bergen, Allégaten 55, 5007 Bergen, Norway

Received 24 August 2004; received in revised form 30 March 2005; accepted 4 April 2005
Available online 23 May 2005

Abstract

Natural gas hydrates are ice-like structures composed of water and gas molecules that have long been a problem in petroleum industry. Heavy cost of alcohol and glycol injection has spurred an interest in called 'kinetic inhibitors' able to slow down the hydrate formation rather than prevent it. Since it is not possible to compare directly the macroscopic effects of different inhibitors on the kinetics of hydrate formation in computer experiments, a scheme capable of culling the list of candidates for experimental testing was proposed earlier [B. Kvamme, G. Huseby, O.K. Førrisdahl, Molecular dynamics simulations of PVP kinetic inhibitor in liquid water and hydrate/liquid water systems, Mol. Phys. 90 (1997) 979–991]. Molecular dynamics simulations were implemented to test several kinetic inhibitors in a multiphase water–hydrate system with rigid hydrate interface. In addition, a long-scale run was implemented for a system where the hydrate was free to melt and reform. Our conclusion that PVCap will outperform PVP as a kinetic hydrate inhibitor is supported by experimental data. We demonstrate that numerical experiments can be a valuable tool for selecting kinetic inhibitors as well as provide insight into mechanisms of kinetic inhibition and hydrate melting and reformation.

Keywords: Molecular modeling; Clathrate hydrates; Kinetic inhibitors; Water; Multiphase system; Interfacial tension

1. Introduction

Clathrate hydrates of natural gases are ice-like structures composed of water molecules encaging guest gas molecules (see Fig. 1). The list of gas molecules capable of forming clathrate hydrates is extensive and includes a number of abundant compounds, from light hydrocarbons to refrigerants to sour gases like carbon dioxide and hydrogen sulfide. Under conditions typical for oil and gas production and transport in colder climates, clathrate hydrates can easily form in pipelines and production equipment. This has long been a problem for oil-and-gas industry. Traditionally, the formation of hydrates is prevented by injecting large volumes (up to 40%) of alcohols and/or glycols into the production streams. The associated high cost of chemicals and environmental cleanup has inspired the interest in different chemicals, 'kinetic inhibitors' able to slow down the hydrate formation rather than make it thermodynamically impossible. Kinetic inhibitors are active in part per million concentrations. Testing of potential kinetic inhibitors involves expensive manipulation of hydrates at high pressures. On the other hand, computers are becoming cheaper and more powerful than ever. If numerical simulations can be used to cull the experimental candidates, molecular dynamics may prove to be a valuable research tool. Another advantage of computer simulations is that one can modify the model molecule, and see how it will affect its performance.

While it is not feasible at present to compare directly the effects of inhibitors on the macroscopic kinetics of hydrate formation, a scheme enabling one to evaluate the relative performance of kinetic inhibitors in a multiphase water–hydrate system was devised and tested [1]. In this work, four monomers of potential kinetic inhibitors are studied under different conditions and modeling setups: PVP (poly(*N*-vinylpyrrolidine), (Fig. 2a), PVCap (poly(*N*-vinylprolac-

* Corresponding author. Tel.: +47 5 5583310; fax: +47 5 5589440.
E-mail addresses: bjorn.kvamme@ift.uib.no (B. Kvamme), tatyana.kuznetsova@ift.uib.no (T. Kuznetsova), kjetilaa@ift.uib.no (K. Aasoldsen).

1093-3263/$ – see front matter © 2005 Elsevier Inc. All rights reserved.
doi:10.1016/j.jmgm.2005.04.001

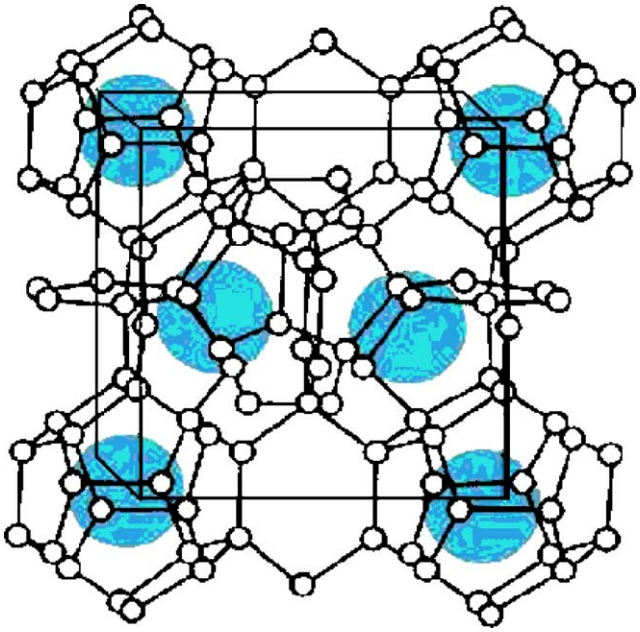

Fig. 1. A unit cell of structure I hydrate. White circles are water; blue spheres are encaged quests.

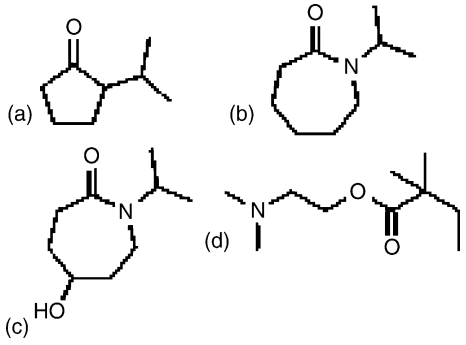

Fig. 2. Ball-and-stick representations of investigated inhibitor monomers: (a) PVCap; (b) PVCap-modified; (c) VC-713. Hydrogens, light blue; oxygens, red; nitrogens are indicated, the remainder atoms, carbons.

tam), (Fig. 2b), a modification of the PVCap monomer, PVCap-modified (Fig. 2c), polymer VC-713 (Fig. 2d).

Two drastically different approaches to molecular modeling of kinetic inhibitor system have emerged so far. Carver et al. and Storr et al. [2–4], set up hydrate surfaces typical for growing hydrate and performed Monte Carlo simulations of kinetic inhibitor chains and active units on these dry hydrate surfaces. On the other hand, Kvamme et al. [1] performed molecular dynamics simulations of a PVP monomer in a composite system of liquid water and a unit hydrate crystal in order to allow the competition between liquid water and hydrate water for the active inhibitor groups to decide the efficiency of a given kinetic inhibitor.

With the hydrate formation, taking place under a surface covered by kinetic inhibitor, or in-between their polymer chain backbone, the hydrate will not form a perfect crystal surface. Furthermore, the presence of liquid water will significantly affect the inhibitor behavior. On a dry surface, the inhibitor segment is completely free to find its path towards the most energetically favorable configuration, regardless of any entropy constraints present in a real system. Hydrate formation and growth in the vicinity of kinetic inhibitor groups will be governed by free energy differences, i.e. not just by energy, but entropy as well. The entropy effects of the polymer backbone, as well other apolar groups in the system will slow down the local water motion, and thus will have dramatic effect on the entropy of the water. In our previous paper [1], it was demonstrated that the PVP monomer had a favorable attachment to the hydrate surface, and that the attachment was also favorable in terms of free energy differences.

2. Methodology

2.1. Simulation details

Our molecular dynamics study involved two sets of molecular dynamics simulations. In order to enable direct comparison, the first simulation setup (Simulation Set I) was identical to our previous investigation of a PVP polymer monomer [1]. Three additional potential kinetic inhibitors were studied as well. They included PVCap, its modification, PVCap-modified, and a polymer referred to as VC-713 by the industry. Simulation setup consisted of a hydrate crystal in contact with liquid water and kinetic inhibitor; it is described in detail in Kvamme et al. [1].

The hydrate–liquid water-kinetic inhibitor system comprised a single unit cell of structure II hydrate [5,6] filled with Freon 11 ($CFCl_3$) molecules, and a liquid phase made of 232 TIP4P [7] water and 41 Freon 11 molecules. Freon molecules were modeled as spherical Lennard–Jones particles (see Ref. [1] for model parameters). The cubic simulation box had 81 liquid water molecules positioned in the top layer, followed by a layer of 64 water and 16 Freon molecules. A unit hydrate cell was placed underneath these two layers. Another 25 Freon molecules composed the layer underlying the hydrate crystal. The remainder of the free water molecules were distributed in-between the hydrate crystal and the simulation box edges. The initial arrangement of liquid water molecules relative to the inhibitor monomers was determined from the conditions of energy minimum and zero dipole moment [1]. Periodic boundary conditions (PBC) were applied in all three directions. Long-range Coulomb forces were treated by Ewald summation technique [8]. The molecular dynamics program was a modified and extended version of the McMoldyn package, originally written by Laaksonen [9].

Simulation set II involved a block of structure I [5,6] methane hydrate made of 20 unit hydrate cells (982 SPC/E water [10] and 144 OPLS one-site methane [11] molecules, see Table 1 for model parameters). The hydrate was first brought into contact with a liquid slab of 862 SPC/E water

Table 1
Model parameters used in this simulation

Site	Atom	σ (Å)	ε (kJ/mol)	Charge, q (Q)
TIP4P H_2O model [7]				
1	O	3.1540	0.6485	0
2	H	0	0	+0.52
2	H	0	0	+0.52
3	PC	0	0	−1.04
SPC/E H_2O model [7]				
1	O	3.1656	0.6502	−0.82
2	H	0	0	0
2	H	0	0	0
United-atom OPLS methane model [11]				
1	C1	3.905	0.7332	0
United-atom OPLS propane model [12]				
1	C 1	3.905	0.7332	0
2	C 2	3.905	0.4940	0
3	C 3	3.905	0.7332	0
PVP and PVCap units				
1	C (ring)[a] connected to O and N	3.800	0.2093	0.380
2	CH_2 (ring)[a] and CH_2 (chain)[c]	3.905	0.4940	0.000
3	CH_2 (ring)[a] connected to N	3.905	0.4940	0.220
4	O[b]	2.905	0.5300	−0.380
5	N[a]	3.320	0.3900	−0.440
6	CH (chain)[a]	3.850	0.3349	0.220
7	CH_3 (chain)[c]	3.775	0.8667	0.000

Charges from [1], LJ parameters: [a][13]; [b][14]; [c][15].

molecules and two inhibitor molecules (monomers of PVP and PVCap, see Table 1 and Fig. 2 for details), and then with a composite water-inhibitor–propane system. The resulting interfacial system used periodic boundary conditions (PBC) in all three directions. PBC results in a simulation box containing two interfaces, a fact that must be taken into account when calculating the interfacial tension in the system, as well as insuring that the system's length in the z direction is long enough to obtain the bulk behavior in the center of both crystal and liquid phases. The interfacial tension (σ) was obtained by a common method using pressure tensor in case where there are two interfaces normal to the z–axis:

$$\sigma = 0.5 \times \overline{h_z}\{P_z - \tfrac{1}{2}[P_x + P_y]\}, \quad (1)$$

where P_i is the average system pressure in the i direction and $\overline{h_z}$ the box length in the direction normal to the interface.

In most of our simulations, the hydrate-forming molecules did not have translational degrees of motion but could still rotate, resulting in a rigid hydrate surface similar to that of [2–4]. The rest of the molecules enjoyed unrestricted motion. A run where all the molecules were free to engage in translational and rotational motion was also produced. This 2 ns-long simulation involved a slowly melting and then reforming hydrate crystal and two active units of PVP polymer.

Molecular Dynamics used the MDynaMix package of Lyubartsev and Laaksonen [16], with explicit reversible integrator for NPT-dynamics of Martyna et al [17], modified by us to implement implicit quaternion treatment of rigid molecules with Nosé-Hoover thermostat for temperature and pressure [18–20]. The time step was set to 0.5 fs. All systems were kept at constant temperature of 261 K and pressure of 7 MPa by means of Nosé-Hoover thermo and barostat. Both experimental and modeling data indicate substantial surface tension in the hydrate–liquid system. Therefore, only tangential components of pressure tensor were used to evaluate and control the pressure, with the MD box allowed to fluctuate in all three directions.

Linux-based message passing interface (MPI) was used to implement parallel computation on either a cluster or standalone dual-processor PCs. The number of processors ranged from 2 to 8. Possible hydrogen bonding was identify by means of distance-angle criterion of the VMD package [21] with the following user-defined parameters: given an atom D with a hydrogen H bonded to it and an atom A with no hydrogen bonded to it, a hydrogen bond exists between A and H if the distance D–A does not exceed 3 Å and the angle D–H–A is less than 24 degrees.

2.2. Inhibitor molecules

Active groups with the most potential for attaching themselves to the hydrate surface include the double-bonded oxygens, the hydroxyl groups, and the nitrogen. Fig. 2 shows that all of our prospective inhibitors possess several of them. The main difference between the PVP and PVCap monomers lies in the fact that the PVCap ring contains two carbons more than the PVP ring (Fig. 2a and b). As

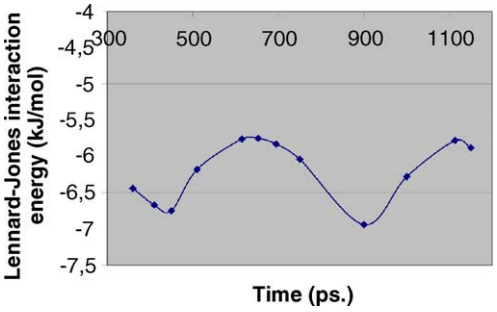

Fig. 3. Lennard–Jones interaction energy for PVCap vs. hydrate water. Indicated rotation with the period of 450 ps.

experiments of Lederhos et al. [22] showed, and simulations presented in this paper confirm, PVCap is superior to PVP when it comes to inhibiting ability. On the other hand, the PVCap ring contains one apolar group more than PVP, and thus expected to be somewhat less soluble in water. With the increased solubility in mind, a modified version of the PVCap monomer has been constructed, with a polar hydroxyl group added to the ring (Fig. 2b).

The active units of polymer VC-713 consist of alternating 5- and 7-rings identical to those of PVP and PVCap, respectively, as well as a third additional active group (shown in Fig. 2d) attached to the paraffin backbone (Fig. 3).

3. Results and discussion

3.1. Simulation set I

In order to achieve comparability, the systems have been run for the same 176 ps as in the PVP simulation of [1]. All starting configurations were also identical to those of the PVP study.

Simulations showed that while both PVP and PVCap monomers tended to position themselves at the hydrate-liquid interface and form hydrogen bonds between the double-bonded oxygen and hydrate water, the attractive interaction with the hydrate is significantly stronger in PVCap than PVP, indicating better attachment and hence more vigorous inhibiting effect (see Table 2). Similar to the PVP situation, correlations between the double-bonded oxygen and hydrogen in liquid and hydrate water change from the initial configuration where PVCap is surrounded by liquid water to the preferred final situation, which is comparable to the final situation for PVP. Experiments [22] also confirm that PVCap is a better kinetic inhibitor than PVP.

Studies of the modified PVCap (PVCap-modified) monomer, for which no experimental data is available, have shown that the insertion of hydroxyl group resulted in increased ring solubility in water. Hydrate water entered into a hydrogen bond with the double-bonded ring oxygen, while the hydroxyl group formed a hydrogen bond with the liquid water. Table 2 shows that despite the drastically differing contributions from electrostatic and Lennard–Jones parts, the average interaction with liquid water for PVCap and PVCap-modified remains roughly the same. On the other hand, the potential energy of the inhibitor–hydrate interaction is significantly lower in case of PVCap monomer, with both Coulomb and Lennard–Jones contributions favoring PVCap-modifed over PVCap. As also illustrated in a previous study [1], the double-bonded oxygen may form hydrogen bonds with more than one hydrate hydrogens at the same time.

As for VC-713, it should be noted that a more realistic picture of the sterical hindrance is needed to rigorously assess its performance as kinetic inhibitor. At present, however, we can state that VC-713 monomer is far more favored energetically to attach to the hydrate surface than either PVP, PVCap or PVCap-modified. Its interaction with the liquid water is weaker than that of any other inhibitors under investigation, and consists almost entirely of short-range interactions.

In summary, when analyzed in conjunction with our previous studies of PVP [1], the computer simulations rank the PVCap-modified above PVCap and PVP when it comes to their expected performance as kinetic inhibitors. The non-ring active group of VC-713 has shown some promising features, but more rigorous conclusions will have to wait for comparison to the extended version of the model.

3.2. Simulation set II

3.2.1. Hydrate–water–PVP/PVCap monomers and dimers

Our composite systems were constructed by placing a rigid hydrate block made of $2 \times 2 \times 5$ structure I units alongside a slab of equilibrated liquid water containing 2 inhibitor monomers, either PVP or PVCap. The initial dimensions of all systems were 24 Å × 24 Å × 106 Å. At the start of the production run, both monomers were positioned 12–15 Å from the hydrate surface. Fig. 4a and b,

Table 2
Properties of composite PVCap and PVCap-modified system

System	PVP			PVCap			PVCap-modified		
Property	Total	Coul.	L–J	Total	Coul.	L–J	Total	Coul.	L–J
Total potential energy (kJ/mole)	−42.71			−43.06			−43.12		
Hydrate water–inhibitor (kJ/mole)	−41.08	−26.01	−15.07	−46.15	−37.51	−8.63	−62.38	−42.48	−19.90
Liquid water–inhibitor (kJ/mole)	−17.02	−9.54	−7.47	−25.77	−8.64	−17.13	−24.56	−19.23	−5.33

'Coul.' stands for electrostatic contributions; 'L–J', short-range Lennard–Jones contributions to the total energy.

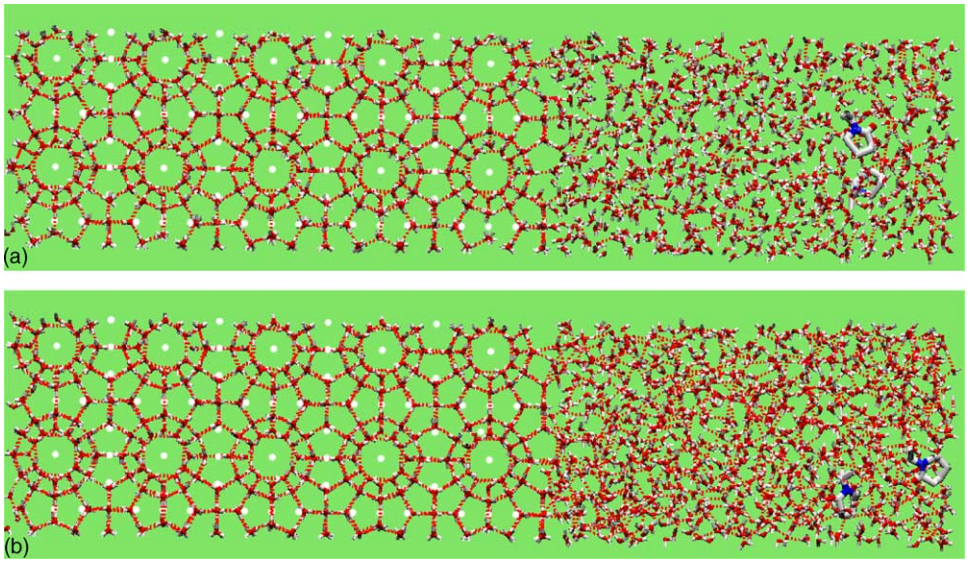

Fig. 4. Evolution of the PVCap–water–propane-hydrate system. Water molecules are red-and-white lines, propanes are cyan lines, PVCaps are cyan, red and blue. (a) The starting configuration. (b) The final configuration: Given the periodic boundary conditions, PVCap molecule to the left remains at the water–hydrate interface. The second PVCap molecule is immersed in propane near the water–propane interface.

made by the VMD package [21], present snapshots of the PVCap–water–hydrate system at the beginning and end of the production run of 1.2 ns. Given the periodic boundary conditions, PVCap molecule at the right edge of the picture is located on the water–hydrate interface. This pattern was shared by both PVP and PVCap-containing systems: one of the two monomers made its way to the hydrate surface, while the other drifted further away into the liquid phase.

On the other hand, when it came to their kinetics and potential energies, the behavior of PVCap monomers was quite different from that of PVP. One important difference lay in the absence of hydrogen bonding between hydrate water molecules and PVP. Another one was the fact that even though PVCap monomers contain a seven-ring (and thus are bulkier than PVPs), one of the PVCap monomers approached the hydrate–liquid interface and positioned itself with its double-bonded oxygen pointing into the liquid water phase after only 250 ps of simulation. It took the PVP monomer almost four times longer (900 ps) to cross the same distance. From 250 ps onward, PVCap the monomer remained on the interface, slowly rotating with the period of 450 ps. Thus the double-boded oxygen was facing the

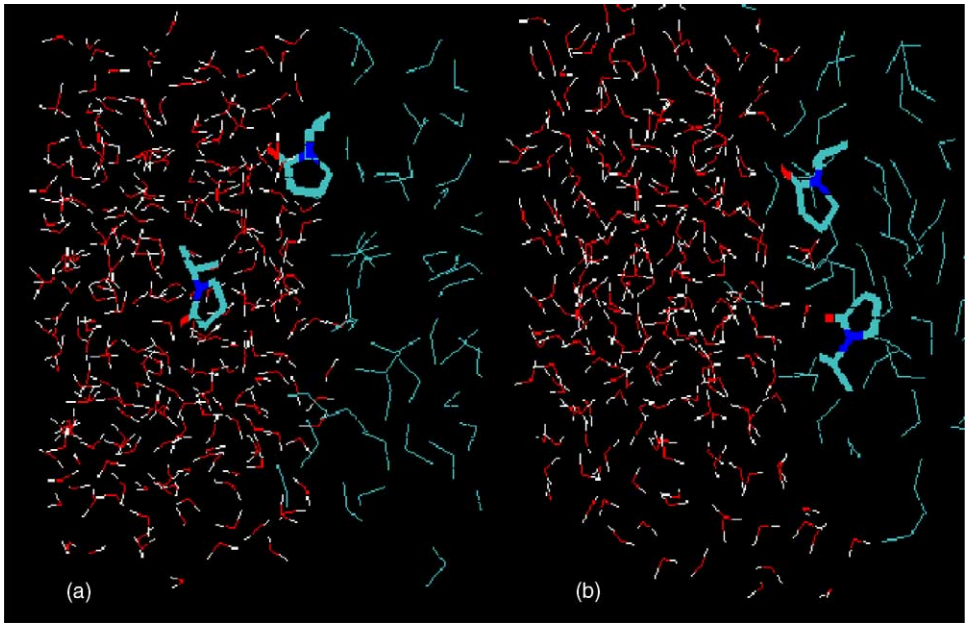

Fig. 5. Evolution of the PVP–water–propane-hydrate system. Water molecules are red-and-white lines, propanes are cyan lines, PVPs are cyan, red and blue. (a) The starting configuration. (b) The final configuration: both PVP inhibitors are partially immersed in propane near the water–propane interface.

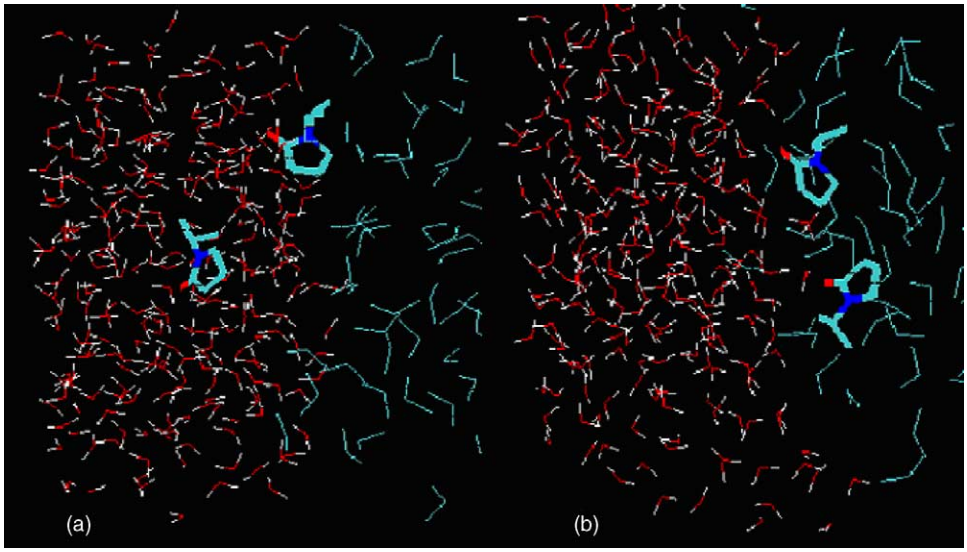

Fig. 6. Evolution of the PVCap–water–propane-hydrate system. Water molecules are red-and-white lines, propanes are cyan lines, PVPs are cyan, red and blue. (a) The starting configuration. (b) The final configuration: Given the periodic boundary conditions, PVCap molecule to the left remains at the water–hydrate interface. The second PVCap molecule is partially immersed in propane near the water–propane interface.

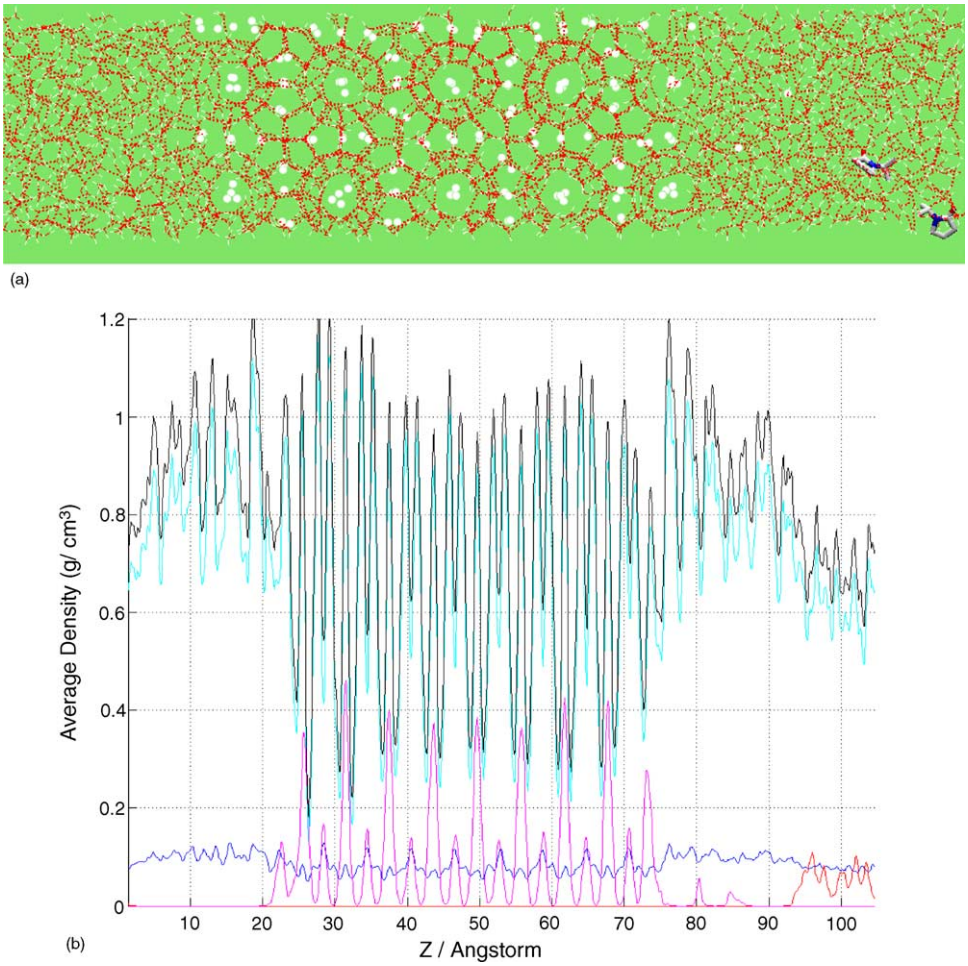

Fig. 7. (a) Snapshot of the freely moving PVP–water–hydrate system approximately 7 ps after the start of the production run. Water molecules are red-and-white lines, methanes are white balls, PVPs are cyan, red and blue. Hydrogen bonds are represented by dashed lines. (b) Mass density profiles corresponding to part (a) configuration. Full lines correspond to smoothed fince-scale profiles; magenta, methane; cyan, oxygen; blue, hydrogen; red, PVP; black is net density. Dashed lines are coarse-grained profiles produced by the first of FIR filters.

hydrate surface and in position to form hydrogen bonds with the hydrate water molecules during the simulation a considerable amount of time. The other PVCap monomer spent the whole of the simulation at varying distances from the hydrate – water interface in the liquid water. The end of the simulation found this monomer in the middle of the liquid phase (Fig. 4b).

The differences between the PVP and PVCap inhibitor monomers are underlined further when one looks at the interaction between them and water molecules belonging to either hydrate crystal or liquid water. Table 2 shows that the potential energy of inhibitor–hydrate interaction is significantly lower in case of PVCap monomer, with both Coulomb and Lennard–Jones contributions favoring PVCap over PVP. As noted, the PVP monomer at the interface never positioned itself to form hydrogen bonds with the hydrate phase within the time frame of the simulation. The interfacial tension in the PVCap system was reduced by about 25% in comparison with that in the PVP system, from 203 to 151 mN/m, indicating PVCap's clear superiority as surfactant.

Systems containing the dimers of PVP and PVCap exhibited behavior much differing from that of their monomers. The dimers stayed close together, the fact we attributed to hydrophobic attraction (borne out by the analysis of methane behavior in another simulation system, see below). Almost no inhibitor movements were detected in the system throughout the whole of the simulation run of about 900 ps. Both PVP and PVCap dimers kept the same distance from the hydrate – liquid water interface, with no inhibitor molecules positioned at the interface.

3.2.2. *Hydrate–water–propane–PVP/PVCap monomers*

In order to investigate the differences between the PVP and PVCap monomers in a multiphase environment typically found in oil-and-gas production and transport, we replaced a part of the liquid water phase by a layer of liquid propane (united atom OPLS model [12], Table 1), creating two competing interfaces (water–hydrate and water–hydrocarbon). Both PVP and PVCap are proven surfactants, and the resulting interface between liquid water and hydrocarbon enabled us to test their relative affinity for the water–hydrate interface. Both PVP monomers quickly approached the propane layer and moved along the propane–water interface monomer, staying close together and never

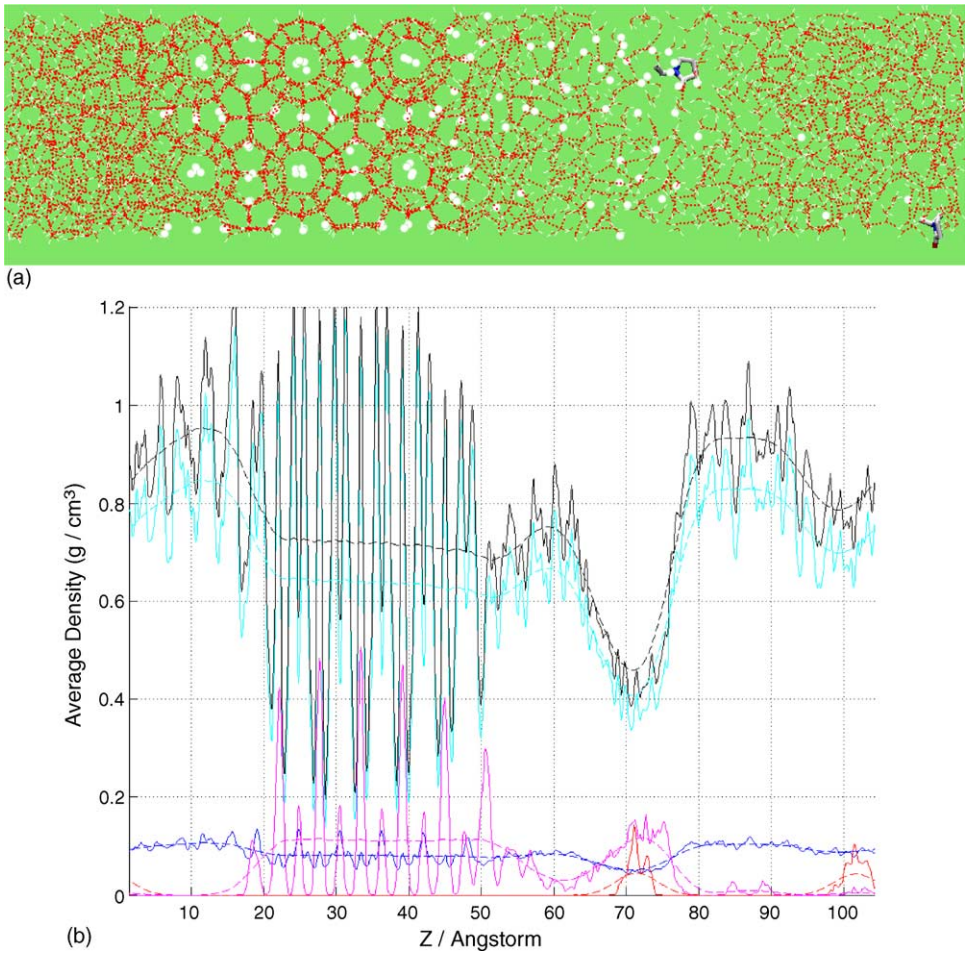

Fig. 8. (a) Same system as in Fig. 7; 0.17 ps elapsed since. Same conventions as in Fig. 7a. (b) Mass density profiles corresponding to part (a) configuration. Same conventions as in Fig. 7b.

entering the propane bulk. These monomers were oriented so their double-bonded oxygens faced the interface and formed hydrogen bonds with different water molecules (Fig. 5a and b). In a sharp contrast to this, the PVCap monomer positioned at the water–hydrate interface at the start of the run remained there and turned around to enable hydrogen bonding with the hydrate, while the other monomer moved to the water–propane interface, fully immersing itself in the propane phase but with the double-bonded oxygen forming hydrogen bonds with water (Fig. 6b).

3.2.3. Freely moving hydrate–water–PVP monomers

The last of simulation setups described in this work provides a fascinating insight into the mechanisms of hydrate formation inhibition and the interplay between various factors determining the behavior of complex interfacial systems composed of clathrate hydrates, liquid water, and organic compounds such as kinetic inhibitors. As opposed to the rest our simulations, where the hydrate-forming molecules could only rotate, forming a rigid hydrate surface, we used a hydrate–water–PVP system of Section 3.2.1, and allowed an unrestricted motion of all the molecules in the production run of 2.5 ns.

The complexity of hydrate structure far surpasses that of ice, due to both the inclusion of guest molecules and two different water structures encaging them (large and small cages) and making up the structure I hydrates (Fig. 1). In the event of hydrate melting, possible under this simulation setup, the additional presence of methane molecules in the liquid phase will complicate the analysis of the system's structural and dynamic behavior even further. We found that the best results were yielded by combining the analysis of mass-density profiles with the visual inspection of the hydrogen bond network (Figs. 7–12).

3.2.3.1. Density profiles and hydrate structure. The density profiles of x–y averaged quantities of interest (mass density and charge density in our case) are generated by partitioning the simulation box into discrete bins in the z direction. We followed the general approach of Davidchak and Laird [23] and applied finite impulse response (FIR) filters [23,24] to produce a smooth coarse-grained profile from the oscillating *fine-scale* profiles. Our system ranged around 105 Å in the z

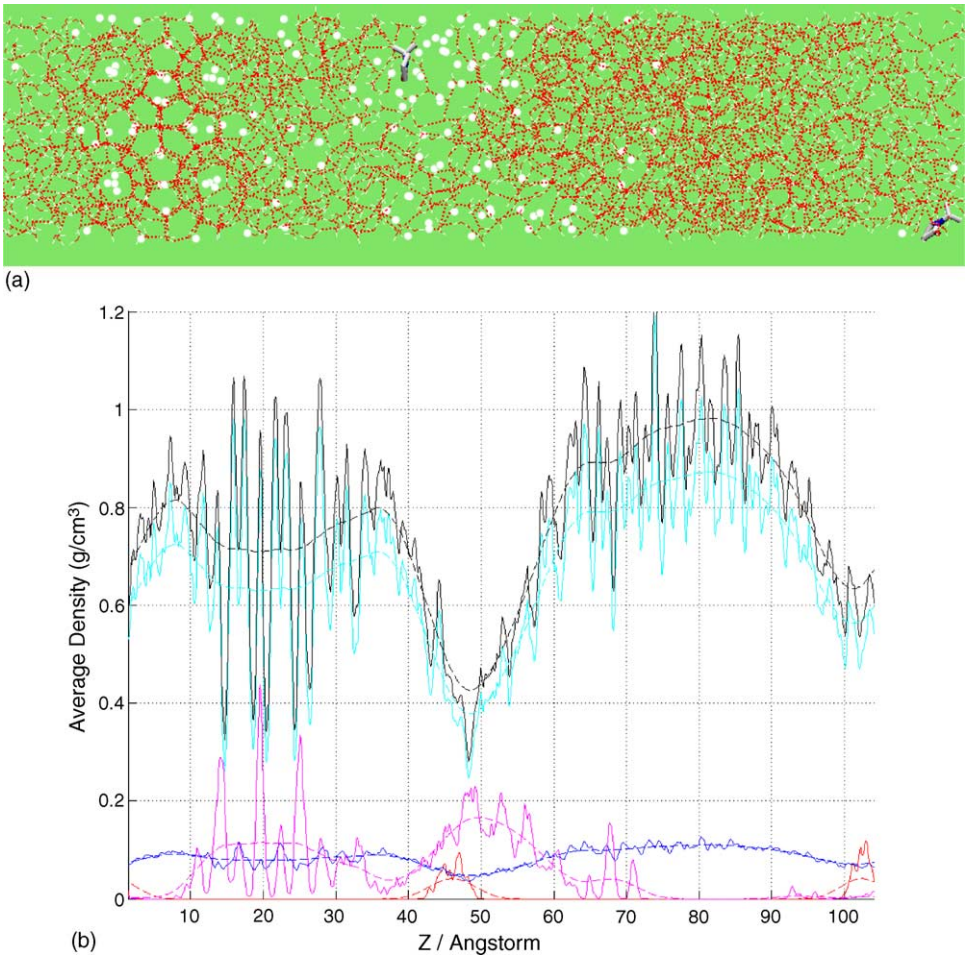

Fig. 9. (a) Same system as in Fig. 8; 0.57 ps elapsed. Same conventions as in Fig. 8a. (b) Mass density profiles corresponding to part (a) configuration. Same conventions as in Fig. 8b.

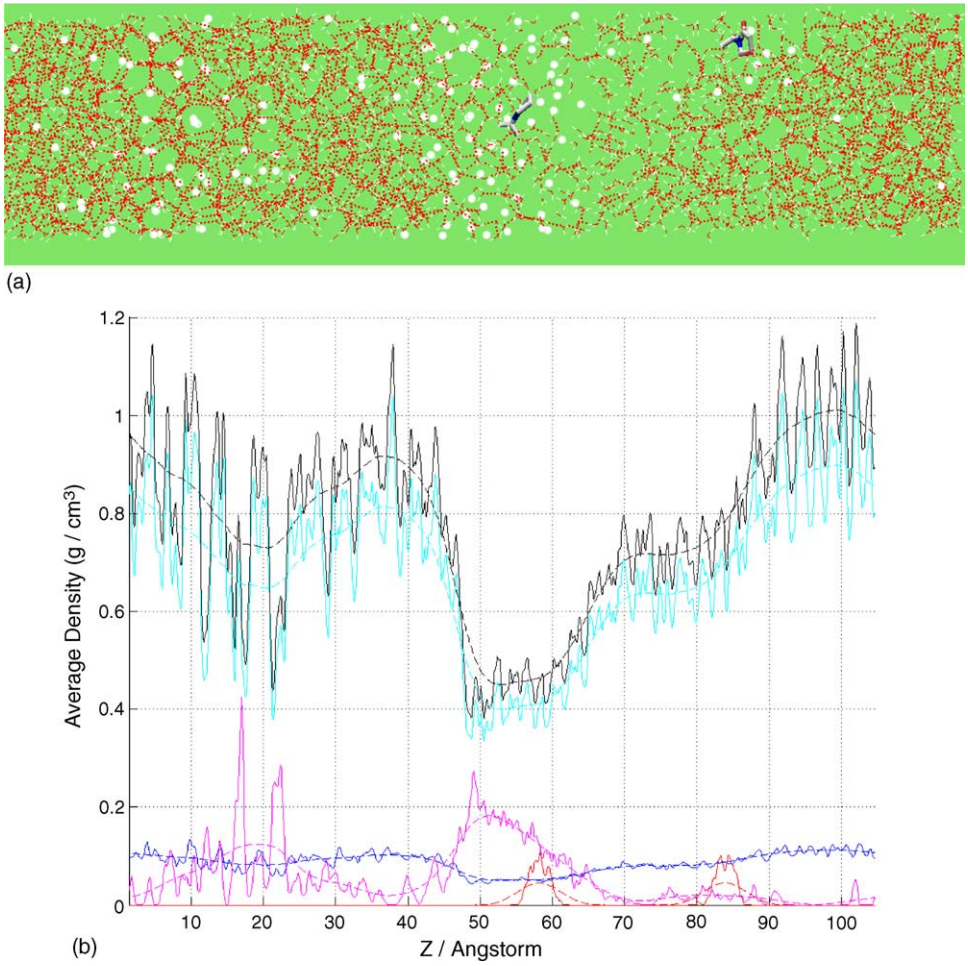

Fig. 10. (a) Same system as in Fig. 8; 0.81 ps elapsed. Same conventions as in Fig. 8a. (b) Mass density profiles corresponding to Fig. 9a configuration. Same conventions as in Fig. 8b.

direction, with the number of bins used to generate the fine-scale profile set to 1200. The filtered profile was obtained from the fine-scale profile f_n as follows [23]:

$$\bar{f}_n = \sum_{k=-N}^{N} w_k f_{n+k} \tag{2}$$

The shape of the filter was assumed to be Gaussian from the outset:

$$w_k = Ae^{-(k/\varepsilon)^2}, \quad k = -N, \ldots, N \tag{3}$$

The normalization constant A was determined from the condition $\sum w_k = 1$. Two filters, each with its own N and ε, were used, the first one aimed to average over the oscillations due to hydrate's layered structure but retain the essential features of the interfacial region. The values of $N = 68$ and $\varepsilon = 42.5$ appeared to satisfy both conditions for our system and were used to generate a coarse-grained profile. The second filter was used to smooth out only the momentary fluctuations in the density profiles while maintaining its oscillatory nature. This filter was much narrower, with $\varepsilon = 2.4$. A technique of window averaging reflecting the hydrate crystal spacing was also tried but failed to produce profiles fluctuating only in the interfacial region similar to those of Bryk and Haymet [24] for ice–water interfaces.

The characteristic structure of a methane hydrate is well represented in Fig. 7 showing the interfacial system approximately 7 ps after the start of the production run. In Fig. 7b, one can clearly see both the alternating high- and low-density peaks of encaged methane guests (full magenta line) and the corresponding spacing of oxygen peaks (full cyan line). The low-density methane peaks coincide with the valleys of oxygen density, the high-density peaks, with the peaks in the oxygen profiles. Another characteristic feature of the hydrate structure is provided by the regular pattern of four hydrogen peaks (full blue line). Two of those hydrogen peaks coincide with the methane peaks, the other two (of equal height) are located just off the oxygen peaks. This highly structured pattern of hydrogen density is totally absent in the liquid water phase and will be utilized in later analysis of hydrate reformation. The liquid phase also includes methane molecules (released by incipient hydrate

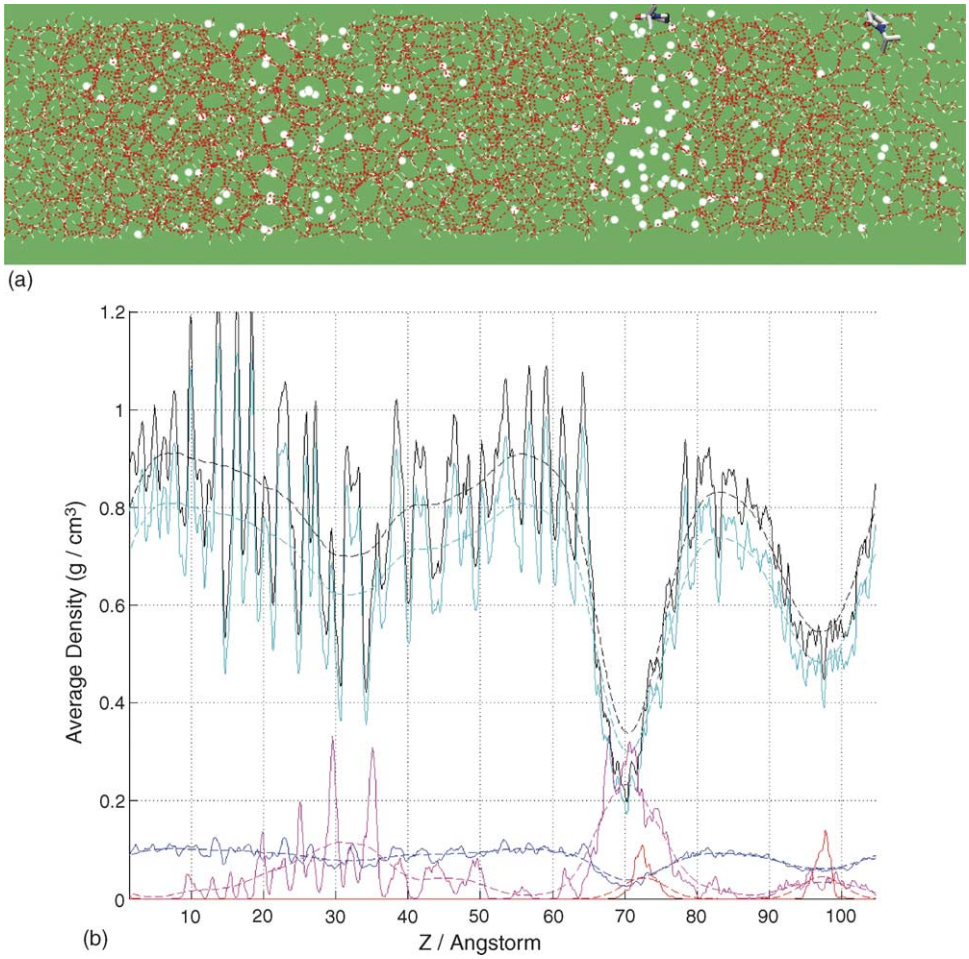

Fig. 11. (a) Same system as in Fig. 8; 1.18 ps elapsed. Same conventions as in Fig. 8a. (b) Mass density profiles corresponding to Fig. 9a configuration. Same conventions as in Fig. 8b.

dissolution), as well as two PVP molecules (full red line). Both fine-scale and coarse-grained profiles of charge density (not shown) proved to be quite unremarkable and were of no help in deciphering the interfacial and bulk structures.

The dashed lines in Fig. 7b are coarse-grained profiles produced by the first of FIR filters. The picture they present is that of the system with a smooth interface between uniform hydrate bulk and liquid water. The 10–90 widths of all filtered density profiles amount to about 8–10 Å. On the other hand, the envelopes of the fine-scale profiles appear to indicate that the existence of the hydrate-liquid interface might manifest itself as local compression/dilation of several hydrate layers and thus reach much further into the hydrate structure than the coarse-grained profiles and theoretical considerations might suggest.

3.2.3.2. System evolution. Thermodynamic stability requires the parity of chemical potential for both water and guest molecules in the hydrate and liquid phases. As a result, the absence of methane in a system comprised by just hydrate and pure water (our starting setup) should give rise to a chemical-potential driving force for hydrate dissolution. On the other hand, as shown by the series of density profiles and snapshots (Figs. 7–12), while it was left undisturbed by the inhibitor, the leftmost water–hydrate interface remained stable, so this force does not play a significant part on the nanosecond time scale, a fact that can be attributed to the low solubility of methane in water.

At the start of the production run, both PVP molecules were positioned closer to the r.h.s. interface at the distance of about 15–18 Å. As shown by the series of snapshots and density profiles in Figs. 7–9, one of the PVP molecules started moving towards the rightmost interface, triggering a rapid dissolution the of hydrate-liquid interface but never coming into direct contact with the hydrate itself; the closest distance of approach was around 12 Å (Fig. 9).

The analysis of this PVP-triggered process of hydrate dissociation made us to conclude that the most persisting hydrate formation at the melting hydrate–water interface appeared to be the ‘half-cage’ structures (guest molecules enclosed by a hydrogen-bonded cage of water molecules typical for hydrate on the one side, and halfway surrounded by a liquid-structured environment on the other side). The hydrate melting itself proceeded in a succession of two

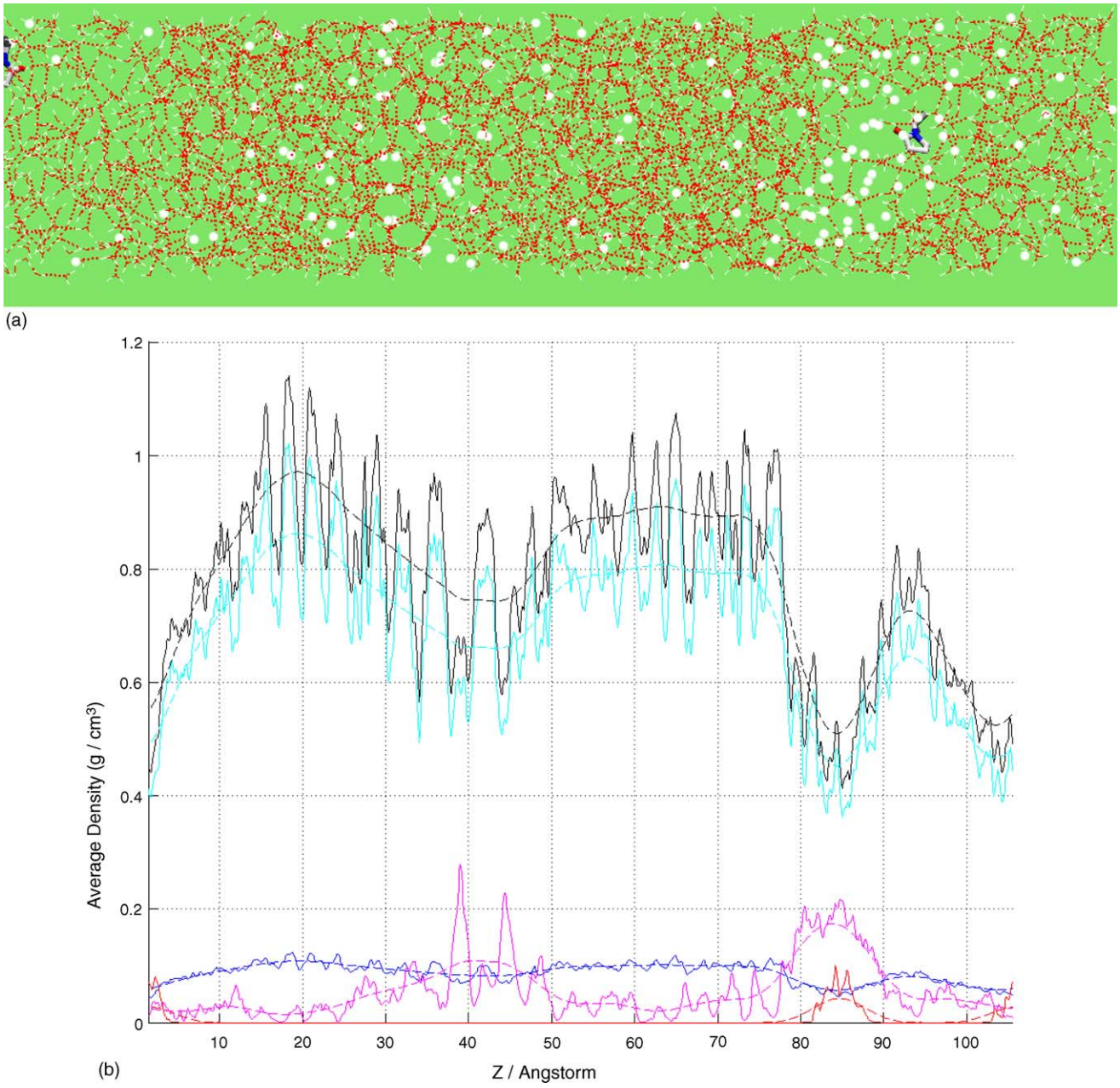

Fig. 12. (a) Same system as in Fig. 8;1.45 ps elapsed. Same conventions as in Fig. 8a. (b) Mass density profiles corresponding to Fig. 9a configuration. Same conventions as in Fig. 8b.

steps: relatively slow dissociation of the half-cages followed by rapid dissolution of the exposed intact layer of hydrate crystal.

Given that the methane content of hydrate exceeds the methane solubility in water by at least two orders of magnitude, methane released by dissociating hydrate will eventually form a bubble (cluster) whose small curvature will increase the water–hydrocarbon interfacial tension and make it even more attractive for surfactants such as PVP (e.g. Fig. 9a). As one can see in Figs. 8–12, the PVP unit showed a strong preference for the water–hydrocarbon interface over the water–hydrate one, thus supporting the findings described in Section 3.2.2, which featured a flat water–propane interface.

The second water–hydrate interface remained stable for over 1.5 ns until the approach of the second PVP once again triggered the fast hydrate dissolution (Figs. 9 and 10). Density profiles in Figs. 10–12 show that just like the first one, the second PVP molecule attached itself to a small cluster of released methane drifting away from the hydrate interface and towards the larger methane bubble. This withdrawal of the PVP molecule appeared to stabilize the remaining hydrate crystal structure, as evidenced by the initial strengthening of methane density peaks in Figs. 10 and 11. Moreover, as both

the density profiles and the system snapshots of Figs. 11 and 12 prove, the liquid phase on the both sides of the hydrate crystal remainder has started to restructure itself into a typical hydrate formation (note the appearance of the fourth methane peak and the distinct cage-like structure of hydrogen bonds around the methane molecules). Note also the distinct pattern of hydrogen density peaks starting to emerge in Figs. 11b and 12b. This rapid restructuring bears all the hallmarks of experimental phenomena often found in hydrate literature [25], the so-called 'hydrate memory' effect, i.e. the fact that when hydrates have been produced from a mixture of water and guest molecules, and then destroyed by changing the conditions, the secondary formation of hydrates will proceed at a much faster rate than the primary one. This observed reformation of hydrates certainly lends weight to our belief that computer simulations can reproduce complex processes occurring in the systems involving hydrates in contact with liquid phases.

The marked preference for water–hydrocarbon interface exhibited by a promising kinetic inhibitor like PVP highlights an important potential problem of industrial inhibitor application. Real-life hydrate-liquid systems will always contain free hydrocarbons due to one cause or another, which will mean a competition for surfactants between the water–hydrate and water–hydrocarbon interfaces. Inhibitors with large specific affinity for the water–hydrate interface are needed, with the affinity provided either by their polar heads or by folding of their carbon backbone over the hydrate surface.

The applicability of the modeling results for the industrial and experimental systems will also be subject to another important consideration: depending on the chain-lengths and chain-length distributions (determined by the polymer production process), the real-life inhibitors may have molecular weights varying in the 10^4 to 10^6 g/mole range. The effects studied here are primarily those of attachment to and dissociation of the hydrate-liquid interface. Factors, such as chain length distribution may also have significant influence in terms of interface coverage and coupling to the forming hydrates.

4. Conclusions

Computer simulations studies of the model systems presented in this paper led us to conclude that PVCap will outperform PVP as a kinetic hydrate inhibitor. A modified version of the PVCap monomer, with a hydroxyl group added to the ring, increased its potential for attachment to the hydrate surface even further. Simulations involving the third active unit of polymer VC-713 (PVP and PVCap being the other two active groups attached to the polymer's backbone) indicated a favorable interaction with the hydrate water as well.

Our over 2 ns-long simulation of a model hydrate–water–PVP system where all the molecules were free to move provided instructive insights into the processes and pathways of hydrate dissociation and reformation in the presence of kinetic inhibitors. We showed that a kinetic inhibitor could apparently trigger the dissolution of hydrate without coming into a direct contact with the hydrate surface. The subsequent withdrawal of the PVP units away from the interfaces was the result of the competition between the hydrate–water and hydrocarbon–water interfaces and the PVPs preference for the latter (much less pronounced in the case of PVCap). Freed from the inhibitor influence, the remaining hydrate crystal provided the nucleus for the process of hydrate reformation, thus mimicking the experimental phenomena of 'hydrate memory'. This complex sequence of events and competing mechanisms exhibited by our model system highlights the interplay between various factors determining the behavior of complex interfacial systems of clathrate hydrates, liquid water, hydrocarbons, and organic compounds. It also strengthens the belief that computer experiments not only provide a feasible way to cull the field of kinetic inhibitors for subsequent experimental testing, but also offer insights into the microscopic mechanisms governing the inhibitor-induced dissociation and reformation of hydrates. Even if we had to extend the procedure to larger polymer segments and bigger computer clusters, computer experiments will still be far less expensive than running high-pressure lab and pilot-scale experiments.

Acknowledgements

Support of Norwegian Supercomputing Project through the grant of CPU time quota is gratefully acknowledged. One of the authors (TK) is grateful to the Norwegian Research Council for the grant of a postdoctoral scholarship.

References

[1] B. Kvamme, G. Huseby, O.K. Førrisdahl, Molecular dynamics simulations of PVP kinetic inhibitor in liquid water and hydrate/liquid water systems, Mol. Phys. 90 (1997) 979–991.
[2] T. Carver, M. Drew, P. Rodger, in: Proceedings of the 2nd international conference on natural gas hydrates, Toulouse, France, June 2–6, 1996, p. 319.
[3] T. Carver, M. Drew, P. Rodger, Faraday Trans. 92 (1996) 5029–5033.
[4] T.M. Storr, P.C. Taylor, J.-P. Monfort, P.M. Rodger, Kinetic inhibitors of hydrate crystallization, J. Am. Chem. Soc. 126 (2004) 1569–1576.
[5] M. von Stackelberg, H.R. Müller, Feste Gashydrate. II. Structur und Raumchemie, Z. Elektrochem. 58 (1954) 25–39.
[6] M. von Stackelberg, W. Jahns, Feste Gashydrate, Z. Elektrochem. 58 (1954) 162–164.
[7] W. Jorgensen, J. Chandrasekhar, J.D. Madura, R.W. Impey, M.L. Klein, J. Chem. Phys. 79 (1983) 926–935.
[8] M.P. Allen, D.J. Tildesley, Computer Simulation of Liquids, Oxford Science Publications, Clarendon Press, Oxford, 1987.
[9] A. Laaksonen, Computer-simulation package for liquids and solids with polar interactions. 1. McMoldyn H20 – aqueous systems, Comp. Phys. 42 (1986) 271–300.

[10] H.J.C. Berendsen, J.P.M. Postma, W.F. van Gunsteren, J. Hermans, in: B. Pullman (Ed.), Intermolecular Forces, Reidel, Dordrecht, 1981.
[11] W.L. Jorgensen, J.D. Madura, C.J. Swenson, Optimized intermolecular potential functions for liquid hydrocarbons, J. Am. Chem. Soc. 106 (1984) 6638–6646.
[12] S.E. DeBolt, P.A. Kollman, Investigation of structure, dynamics, and solvation in 1-octanol and its water-saturated solution – molecular-dynamics and free-energy perturbation studies, J. Amer. Chem. Soc. 117 (1995) 5316–5340.
[13] A. Maliniak, A. Laaksonen, J. Korppitommola, Molecular-dynamics simulation study of associations in aqueous-solutions of quinuclidine, J. Am. Chem. Soc. 112 (1990) 86–93.
[14] C.A. English, J.A. Venables, Structure of diatomic molecular solids, Proc. Royal Soc. London Ser. A: Mathemat. Phys. Eng. Sci. 340 (1974) 57–80.
[15] S. Toxvaerd, Molecular-dynamics calculation of the equation of state of alkanes, J. Chem. Phys. 93 (1990) 4290–4295.
[16] A.P. Lyubartsev, A.M. Laaksonen, DynaMix: a scalable portable parallel MD simulation package for arbitrary molecular mixtures, Comp. Phys. Commun. 128 (2000) 565–589.
[17] G.J. Martyna, D.J. Tobias, M.L. Klein, Constant-pressure molecular-dynamics algorithms, J. Chem. Phys. 101 (1994) 4177–4189.
[18] S. Nosé, Constant temperature molecular-dynamics methods, Progr. Theor. Phys. Suppl. 103 (1991) 1–46.
[19] W.G. Hoover, Canonical dynamics: equilibrium phase-space distributions, Phys. Rev. A 31 (1985) 1695–1697.
[20] D. Fincham, Leapfrog rotational algorithms, Mol. Simul. 8 (1992) 165–178.
[21] W. Humphrey, A. Dalke, K. Schulten, VMD: visual molecular dynamics, J. Mol. Graphics 14 (1996) 33–38.
[22] J.P. Lederhos, J.P. Long, A. Sum, R.L. Christiansen, E.D. Sloan, Effective kinetic inhibitors for natural gas hydrates, Chem. Eng. Sci. 51 (1996) 1221–1229.
[23] R.L. Davidchack, B.B. Laird, Simulation of the hard-sphere crystal–melt interface, J. Chem. Phys. 108 (1998) 9452–9462.
[24] T. Bryk, A.D.J. Haymet, Ice 1 h/water interface of the SPC/E model: Molecular dynamics simulations of the equilibrium basal and prism interfaces, J. Chem. Phys. 117 (2002) 10258–10268.
[25] E.D. Sloan, Clathrate Hydrates of Natural Gases, 2nd ed., Marcel Dekker, New York, 1998.